Controlling and tracking the maximum active power point in a photovoltaic system connected to the grid using the fuzzy neural controller

Ziyodulla Yusupov[1], Elnaz Yaghoubi[1] and Elaheh Yaghoubi[1]

[1]Department of Electrical-Electronics Engineering, Faculty of Engineering, Karabuk University, Karabuk, Turkey
ziyadullayusupov@karabuk.edu.tr, 2138171014@ogrenci.karabuk.edu.tr, 2138171007@ogrenci.karabuk.edu.tr

Abstract

In contemporary smart distribution microgrids, both AC and DC loads and sources are consistently accessible, often operating at varying voltage levels simultaneously. Consequently, the typical scenario in today's microgrids involves a hybrid microgrid setup, necessitating the integration of inverters to facilitate power sharing between the AC and DC sections. Hence, this paper introduces a solution for active power control within an integrated AC/DC microgrid incorporating decentralized photovoltaic sources. The proposed solution employs a fuzzy neural controller to manage power generation, including the complexities of tracking the maximum power point during partial shading conditions. This approach effectively addresses the challenges posed by the combined microgrid configuration. The simulation results provide clear evidence of the success of the proposed method in controlling the active power managed by the DC microgrid and transferring it to the AC section.

1. Introduction

The increasing use of distributed generation (DGs) and renewable energy sources has made their effective management essential to enhance reliability, minimize losses, etc [1]. Microgrids (MGs) can be categorized into three types based on their structure and function: AC, DC, and AC-DC MGs [2]. The islanded MGs configuration is commonly used in remote areas where the national grid is inaccessible [3]. Given that the majority of renewable energy sources generate direct current (DC), while electronic and control devices like induction motors, computers, and communication equipment require DC voltage, researchers suggest the use of DC MGs to increase system efficiency [4]. However, the transformation of the network from AC to DC is not currently financially feasible due to the AC established structure in the distribution network and the widespread adoption of AC-input electrical devices. Ongoing research in this area encompasses energy management, power quality, interface converter, and related fields [5]. Moreover, many studies have been conducted in optimal power distribution [6]. Most endeavors focused on optimizing MGs distribution and management have primarily centered around implementing demand response strategies [7].

2. Grid-Connected Controllable Inverter

The article discusses a bidirectional AC/DC inverter converter that samples voltage and current at the grid connection point. These values are then processed in a synchronized reference frame transformation unit to determine reference voltage and current. Voltage and current controllers use error-values to continuously minimize discrepancies, ensuring convergence with the reference values. A fuzzy neural controller is crucial in maintaining the photovoltaic system's output voltage by adjusting the reference id. It utilizes expert system and input-output alteration diagrams, and transfers reference voltage to the AC network through the MPPT control block. Additionally, the article highlights the design of an ANFIS controller using MATLAB's Fuzzy Logic Toolbox. The NSC controller, operating in dq coordinates, regulates DC link voltage and injects reactive power into the grid or controls voltage at the PCC. This control strategy resembles a STATCOM and provides grid support during non-generation periods, a significant advantage of this approach.

In this modeling, the formulated equations for the network side are presented as follows:

$$v_d = -(R_f i_d + L_f \frac{di_d}{dt}) + \omega_n L_f i_q + v_{nd} \qquad (1)$$

$$v_q = -(R_f i_q + L_f \frac{di_q}{dt}) - \omega_n L_f i_d + v_{nq} \qquad (2)$$

In the equations, $L_n, L_f, R_n,$ and R_f represent the filter resistance, network resistance, filter inductance, and network inductance, respectively. Additionally, i_{dq}, v_{ndq} , and $v v_{dq}$ correspond to the d and q components of the point of common coupling (PCC) bus voltage, voltage, voltage source converter (VSC) output voltage, and current transferred to the network. The network's angular velocity, denoted as ω_m, is calculated using the phase-locked loop (PLL). The inner (current control loop) is designed based on the following equations [30].

$$\begin{cases} v_d^* = -v_d^{'} + \omega_n L_f i_q + v_{nd} \\ v_q^* = -v_q^{'} - \omega_n L_f i_d \end{cases} \qquad (3)$$

The NSC (Network Side Converter) controller is designed based on the *d-q* components of the stator current and comprises two control loops. The controller is structured using a cascaded approach, where the inner loop should be faster to track the

changes in the outer loop. The inner loop controls the current components iq and id, while the outer loop controls the DC link voltage. This control scheme controls both reactive power and DC link voltage independently. Since the unit power factor assumption is made (Q=0), the DC link is modeled dynamically using the nonlinear equation (4).

$$\frac{dV_{DC}^2}{dt} = \frac{2}{C}P_t - \frac{2}{C}P_{loss} - \frac{2}{C}\left(P_n + \left(\frac{2LP_n}{3V_{nd}^2}\right)\frac{dP_n}{dt}\right) + \frac{2}{C}\left(\left(\frac{2LQ_n}{3V_{nd}^2}\right)\frac{dQ_n}{dt}\right) \quad (4)$$

Where $P_t, P_n,$ and P_{loss}represent the photovoltaic system's output active power, delivered active power to the grid, and power losses, respectively. Additionally, Q_n stands for the reactive power delivered to the grid, and C represents the capacitance of the DC link .for control design purposes and simplification, the equation is linearized and simplified according to equation (5).

$$\frac{dV_{dc}}{dt} = \frac{1}{CV_{DC}}P_t - \frac{1}{CV_{DC}}P_n \qquad (5)$$

As evident from equation (5), if the output power of the photovoltaic system and the delivered power to the grid are equal, the DC link voltage will remain constant.

1 blank line using 9-point font with single spacing

Table 1. Comparison of Silicon Solar Cell Characteristics at 25 degrees Celsius

Temperature Coefficient of Current	$\alpha = 0.002086[A/C^\circ]$
Temperature Coefficient of Voltage	$\beta = 0.0779[V/C^\circ]$
Reverse Saturation Current	$I_s = 0.5 \times 10^{-4}[A]$
Short-Circuit Current	$I_{SC} = 2.926[A]$
Cell Resistance	$R_S = 0.0277[\Omega]$
Cell Material Coefficient	$\lambda = 20.41[V^{-1}]$

3. Discussion and Analysis of Simulation Results

In this section, to test and validate the proposed method, the simulation of the algorithm introduced for controlling the active power output of a photovoltaic system connected to the AC MG while simultaneously tracking the point of maximum solar power reception under varying radiation and temperature conditions is discussed. The first part of the simulation will examine the proposed method under uniform radiation and temperature conditions. In contrast, the second part will evaluate the proposed method under partially shaded conditions.

3.1. Evaluating the Proposed Algorithm under Uniform Radiation and Temperature Conditions

Performance of Proposed Algorithm under Uniform Radiation and Temperature Conditions. The performance of the proposed algorithm in tracking the point of maximum solar power reception under uniform radiation and temperature conditions is investigated. "Fig. 1" depicts the simulated circuit, which includes the GSA algorithm, fuzzy neural controller, and solar panel. The GSA algorithm determines the voltage corresponding to the maximum power point for each simulation time step, and the fuzzy neural controller adjusts the switching duty cycle to change the solar panel's output voltage.

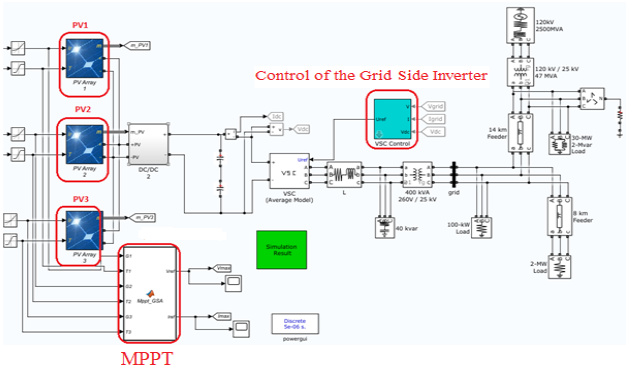

Fig. 1. Schematic of MPPT Circuit under Uniform Radiation and Temperature Conditions

1 blank line using 9-point font with single spacing

"Fig. 2" shows that the temperature and radiation received by each of the three areas of the solar panel remain uniform and consistent, ensuring consistent radiation and temperature conditions for the solar panel. The received radiation and temperature of the solar panel decrease from 1000 W/m² and 40°C to 200 W/m² and 20°C within 1.6 seconds, then increase to 700 W/m² and 30°C within 2.5 seconds. As depicted in the third part of "Fig. 2", with the changing radiation and temperature every second, the output power of the DC and AC segments closely follows the reference maximum power point with high accuracy and speed.

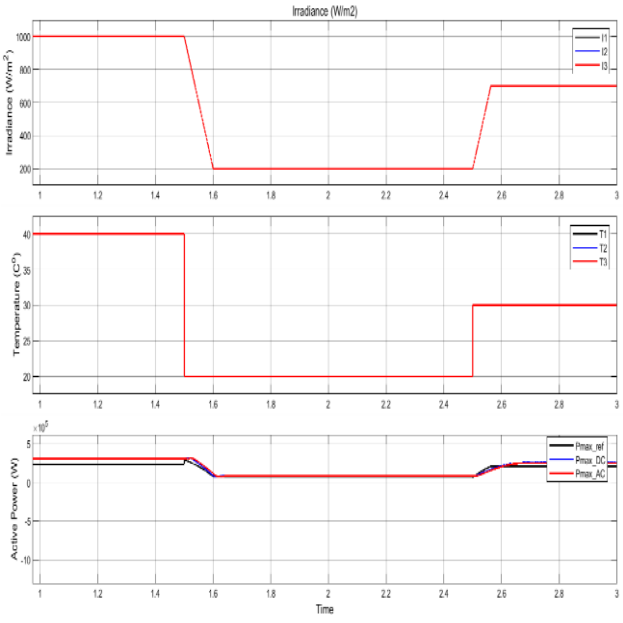

Fig. 2. MPPT Tracking and Corresponding Voltage under Uniform Radiation and Temperature Conditions

"Fig. 3" illustrates the voltage and current variations of the photovoltaic system's output at the connection point to the grid. This issue indicates the appropriate and desirable performance of the phase controller in maintaining the DC link voltage and the control circuit of the AC inverter at the connection point to the grid.

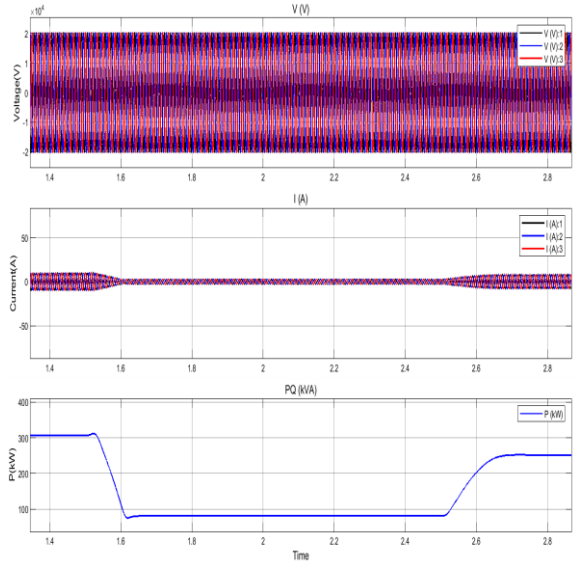

Fig. 3. Voltage, current, and active power changes of photovoltaic system in AC section

"Fig. 4" illustrates the power variations for each section of the photovoltaic system with consistent radiation and temperature changes in each area. Due to the uniformity of input radiation and temperature in each segment, the output power of all three sections remains equal, and their sum corresponds to the tracked maximum power.

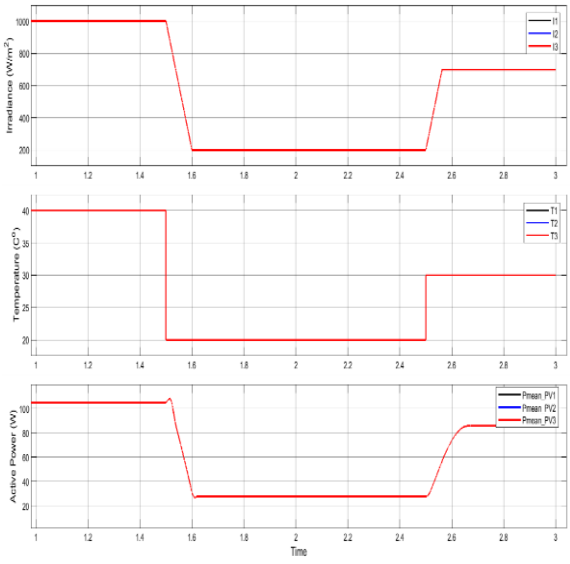

Fig. 4. Active power characteristics of each section of the photovoltaic system under uniform radiation and temperature conditions

4. Review of the Proposed Algorithm in Partial Shade

The proposed algorithm is tested and validated under partial shading conditions using the simulated circuit shown in "Fig. 5" within the MATLAB/Simulink environment. The solar module in the circuit consists of three sections exposed to varying radiation levels and temperatures.

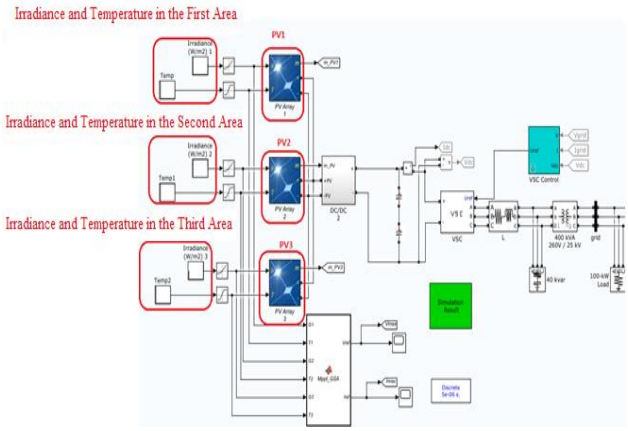

Fig. 5. Electrical circuit for testing and validating in MATLAB/Simulation

In "Fig. 6" is illustrated active power characteristics under rapid radiation and ambient temperature changes for three different sections of solar panels in DC and AC sections. As observed in the figure, the proposed GSA algorithm swiftly and accurately adjusts the panel's voltage and power output toward the maximum voltage and power points.

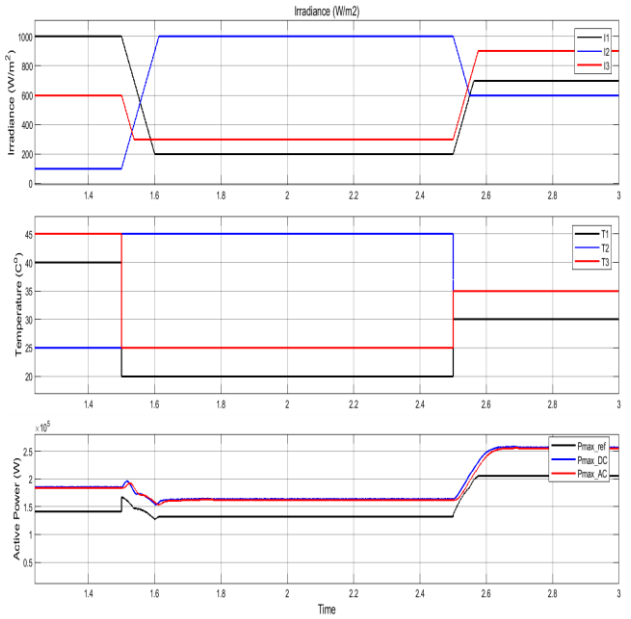

Fig. 6. Active power characteristics under rapid radiation and ambient temperature changes for three different sections of solar panels in DC and AC sections

The fuzzy neural controller in conjunction with the inverter control transfers the obtained maximum power from the DC section to the AC MG. "Fig. 7" illustrates the voltage and current output variations of the photovoltaic system at the connection point to the grid. The changes in power, voltage, and current in this figure demonstrate the appropriate and desirable performance of the fuzzy neural controller in maintaining the DC link voltage and controlling the AC inverter circuit when connected to the grid.

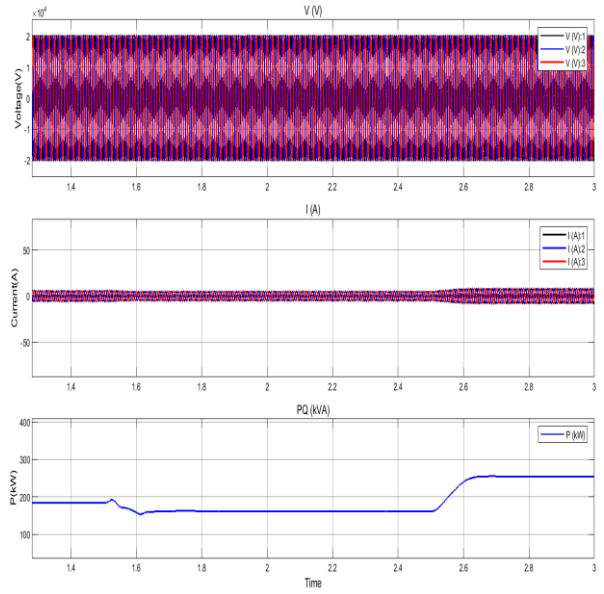

a)

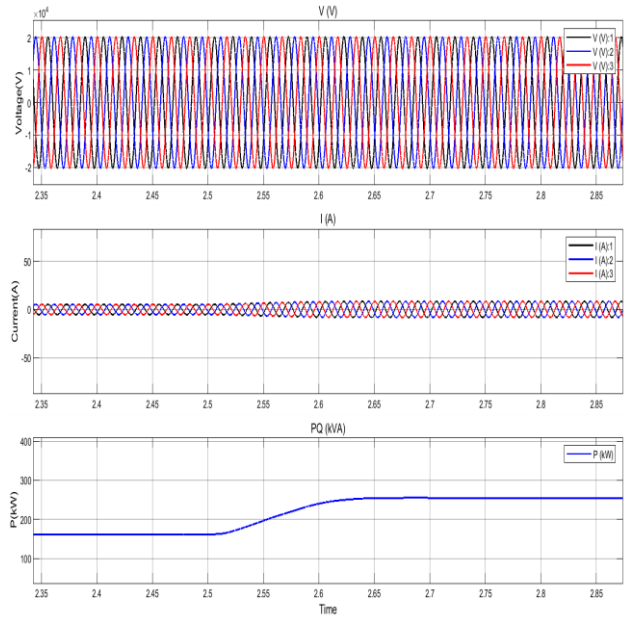

b)

Fig. 7. Variations in voltage, current, and output power in the AC section of the Photovoltaic Panel (a); Grid connection point under rapid changes in solar radiation and ambient temperature (b).

"Fig. 8" depicts the variations in power for each section of the photovoltaic system with changes in solar radiation and temperature in each area. As observed in this figure, due to varying input solar radiation and temperature in each section, the output power of all three sections is different. Yet, their sum corresponds to the maximum tracking power.

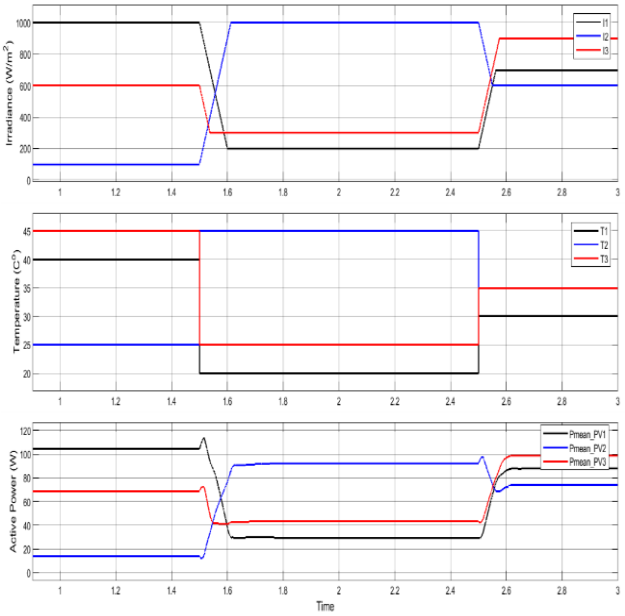

Fig. 8. Changes in the output power of each section of the Photovoltaic system under partial shading conditions

"Fig. 9" A comparison between the proposed method and a PID controller shows that the proposed method based on the fuzzy neural controller exhibits better speed and accuracy in controlling the power at the inverter-grid connection point.

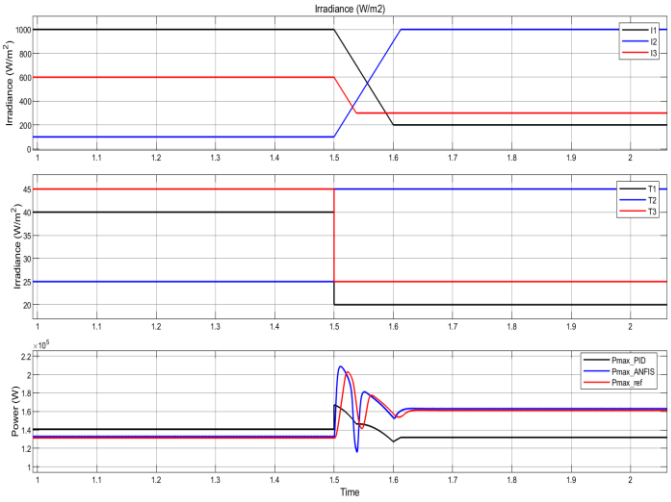

Fig. 9. A comparison between the fuzzy neural controller and PID controller in tracking the maximum power point

In the following, the speed and accuracy of the proposed method in controlling the tracked power under partial shading conditions are compared with a PID controller. The PID controller's control coefficients are optimally selected using various algorithms. As "Fig. 9" shows, the PID controller exhibits a

much more significant delay and significantly lower accuracy in tracking the maximum power point when the incident irradiance and temperature change. This is in contrast to the fuzzy neural control.

In Table (2), a comparison has been made between the PID controller and the suggested approach. As observed in this Table, the proposed method based on the fuzzy neural controller exhibits better speed and accuracy in controlling the power at the inverter-grid connection point.

Table 2. Comparison of the proposed method with other optimized power control algorithms

Studied Method	Accuracy (percentage)	Convergence Time (seconds)
Proposed Neuro-Fuzzy Method	96	0.2
Optimized PID Method Using Genetic Algorithm	92	0.38
Optimized PID Method Using Particle Swarm Optimization Algorithm (PSO)	94	0.25
Conventional Fuzzy Method	95	1.2

5. Conclusions

This paper introduces and models a proposed inverter aimed at active power control by integrating distributed photovoltaic sources into a MG. This control is achieved through the utilization of a fuzzy neural controller. The modelling involved a DC/AC inverter for active power control. The inverter utilized a fuzzy neural controller on the grid side, which is responsible for controlling active power. Additionally, this controller had an inner loop that effectively maintained the DC link voltage at a constant value and minimized disturbances on the DC link, consequently minimizing fluctuations and oscillations on the AC output voltage of the inverter.

Another advantage of this controller was its ability to mitigate the mutual effects of different electrical components, reducing potential damages caused by disturbances between them. Furthermore, the controller's performance tracking the maximum power point under various conditions, including partial shading scenarios, was evaluated and discussed. Outcome of simulations demonstrated the effectivity and capability of the suggested inverter in controlling active power in a MG containing distributed photovoltaic sources.

6. References

[1] Z. Yusupov, E. Yaghoubi, ve V. Soyibjonov, “REDUCING THE VULNERABILITY IN MICROGRID POWER SYSTEMS”, Sci. Innov., c. 2, sayı A5, ss. 166–175, 2023.

[2] L. Ortiz, R. Orizondo, A. Águila, J. W. González, G. J. López, ve I. Isaac, “Hybrid AC/DC microgrid test system simulation: grid-connected mode”, Heliyon, c. 5, sayı 12, 2019.

[3] M. Bhadu, B. Rathor, K. L. Agarwal, S. K. Bishnoi, ve O. P. Mahela, “A Performance Analysis on Robust Primary Control of AC Microgrid with Mitigation of Measurement Noise”, içinde Deregulated Electricity Market, Apple Academic Press, 2022, ss. 179–200.

[4] Y. Liu vd., “A Novel Integral Reinforcement Learning-Based Control Method Assisted by Twin Delayed Deep Deterministic Policy Gradient for Solid Oxide Fuel Cell in DC Microgrid”, IEEE Trans. Sustain. Energy, c. 14, sayı 1, ss. 688–703, 2022.

[5] P. Singh, N. Anwer, ve J. S. Lather, “Energy management and control for direct current microgrid with composite energy storage system using combined cuckoo search algorithm and neural network”, J. Energy Storage, c. 55, s. 105689, 2022.

[6] E. Grover-Silva, M. Heleno, S. Mashayekh, G. Cardoso, R. Girard, ve G. Kariniotakis, “A stochastic optimal power flow for scheduling flexible resources in microgrids operation”, Appl. Energy, c. 229, ss. 201–208, 2018.

[7] S. A. Muaddi ve C. Singh, “Reliability constrained optimal sizing and examining capacity credit and alternatives for renewable energy sources”, IEEE Access, c. 10, ss. 71133–71142, 2022.